Velocity relationships of isolated galaxy pairs in support of MOND-type theories

A. Raymond Penner[1,2]*
[1]Department of Physics, Engineering & Astronomy, Vancouver Island University, 900 Fifth St., Nanaimo, BC, Canada, V9R5S5
[2]Correspondence address: 1544 Scarlet Hill Rd., Nanaimo, BC, Canada, V9T1J3

ABSTRACT

The MOND-type theories of AQUAL (AQUADratic Lagrangian) and GRAS (GRavitational Anti-Screening) are applied to isolated galaxy pairs. Theoretical relationships between their intervelocities, line-of-sight velocities, and their baryonic masses will be derived. These relationships will be compared with observations taken of a set of 3970 highly isolated pairs. The theoretical velocity relationships and distributions provided by AQUAL and GRAS are found to be in very good agreement with these observations. This agreement indirectly implies that there is no fall off in the rotational curves of galaxies, which remain flat out to large distances.

Key words: Gravitation – Galaxies: general – Galaxies: kinematics and dynamics – Galaxies: groups: general – Cosmology: dark matter

1 INTRODUCTION

It has been nearly 100 years since the existence of dark matter was hypothesized (Zwicky 1933). Since then, dark matter has risen from hypothesis to an accepted theory and is an integral part of current cosmological theory, even though dark matter itself remains an enigma. The theory of dark matter has had its greatest success with large-scale structures. For example, models of the distribution of dark matter match well with what is required to explain the hydrostatic stability of hot X-ray emitting intracluster gas, the dominant source of baryonic mass for clusters. In this case, on the order of 5 times more mass is needed than is provided by the baryonic mass of the cluster, which matches well the ratio estimated from the cosmic background radiation (Planck 2020). Of course, dark matter is a very flexible theory in that there is almost no restriction on how much dark matter a galaxy or any specific cluster of galaxies can be taken to contain. The best evidence for dark matter is the gravitational lensing map of the Bullet cluster, where the peak of the lensing map is centred on the galaxies and not on the intracluster gas (Angus et al. 2007).

*Contact e-mail: raymond.penner@viu.ca

Despite its flexibility and its success with clusters, the theory of dark matter has had difficulty dealing with observations on the scale of galaxies. This includes the speed of galactic bars in disc galaxies (Roshan et al. 2021), the distribution of satellite galaxies (Pawlowski 2021), and the prediction that some types of dwarf galaxies should not contain dark matter (Kroupa 2014). A summary of these and other issues can be found in Banik&Zhao (2022). These observations are in serious tension with the theory of dark matter. There is one observation in particular that the theory of dark matter has difficulty with, namely regularities in the rotational curves of spiral galaxies. The observed rotational curves of spiral galaxies are found to flatten out and approach a constant value in their outer regions, with no apparent cut-off to this observation (Famaey&McGaugh 2012). This is a very definitive observation and modeling of the expected dark matter distribution leads to a rotational profile (Navarro et al. 1996,1997) that does not naturally lead to this result (Wu&Kroupa 2015; Desmond 2017a,b). Going beyond just the rotational curves flattening out, it was further found that there is a direct correlation between a galaxy's baryonic mass and this constant outer rotational speed. This again does not fall out from the theory of dark matter. This relationship is known as the Baryonic Tully Fisher Relationship (BTFR) (McGaugh et al. 2000; McGaugh 2012) and is given by

$$M_{bary} = A_{BTFR} v_f^4 \tag{1a}$$

where v_f is the velocity in the outer flattened section of a given spiral galaxy's rotation curve, M_{bary} is the baryonic mass of the galaxy, and A_{BTFR} is a fitted parameter. The value of A_{BTFR} as given by McGaugh (2012) is

$$A_{BTFR} = (47 \pm 6) M_\odot \, km^{-4} s^4. \tag{1b}$$

Recently the relationship between a galaxy's baryonic mass and its rotational speed has been expanded to consider the complete rotational curve. This is highlighted by the work of McGaugh et al (2016) and Lelli et al (2017) who determined the relationship between the radial acceleration as determined from the observed rotational curves and the predicted radial acceleration due to the Newtonian gravity from the determined baryonic mass distribution of the galaxies. The following Radial Acceleration Relationship (RAR) was found to provide a very good fit to the data:

$$g = \frac{g_N}{1 - e^{-\sqrt{g_N/g_o}}}, \tag{2}$$

where g is the true acceleration as determined from the observed rotational curve, g_N is the Newtonian gravitational field as determined from the baryonic mass distribution, and g_o is a

fitted parameter. From McGaugh et al's (2016) data set and their adopted stellar mass-to-light ratio, the fitted value of this observational parameter was found to be

$$g_o = (1.20 \pm 0.02)\ \mathrm{x}\ 10^{-10}\mathrm{ms}^{-2}. \quad (3)$$

In the limit where $g_N << g_o$, (2) leads to

$$g = (g_N g_o)^{1/2}. \quad (4)$$

The value for g_N in (4) needs to take into account that the measurements are taken within the disc of a given galaxy. The required geometric correction leads to

$$g_N = \frac{\alpha G M_{bary}}{r^2}, \quad (5)$$

where $\alpha = (0.76)^{-1}$ (McGaugh&Blok 1998). Therefore, by (4) and (5), in the limit where $g_N << g_o$,

$$g = \frac{\left(\alpha G M_{bary} g_o\right)^{1/2}}{r}\ . \quad (6)$$

The observational BTFR and RAR therefore indicate that at small g or large r, the gravitational acceleration falls off as 1/r rather than the Newtonian $1/r^2$. Substituting $g = v_f^2/r$ into (6) then leads to

$$M_{bary} = A_{RAR} v_f^{\ 4}, \quad (7a)$$

namely the BTFR, with

$$A_{RAR} = (\alpha G g_o)^{-1} = (47.7 \pm 0.8) M_\odot \mathrm{km}^{-4}\mathrm{s}^4, \quad (7b)$$

in agreement with (1).

It is the inability of the dark matter theory to naturally explain the BTFR, and now the RAR, that has been a primary motivation behind alternative theories to dark matter. Both the BTFR and the RAR strongly suggest that it is the baryonic mass of a galaxy that is responsible for the total gravitational force that it experiences. This leads to two general possibilities.

The first possibility is that it is Newtonian theory that needs to be modified. This falls broadly under MilgrOmiaN Dynamics (MOND; Milgrom 1983a,b,c; Berkenstein & Milgrom 1984; Famaey & McGaugh 2012; Sanders 2014; Banik & Zhao 2022). MOND initially involved a modification of the law of inertia, which led to an equation that matches in form with the BTFR. However, modified inertia theories of MOND have been falsified at 6.9σ confidence (Chae 2022). An alternative to this path is to leave the law of inertia intact and instead modify gravitational theory. AQUAL (AQUADratic Lagrangian), a gravitational theory spawned by

MOND, falls under this category (Bekenstein and Milgrom 1984). AQUAL leads to a field equation that reduces to the MOND result in the spherically symmetric case and thereby agrees with the BTFR.

The second possibility for why the baryonic mass would seem to be so tightly correlated with the larger than expected gravitational fields is that baryonic mass itself is directly or indirectly responsible for an additional contribution to the gravitational field. GRAS (GRavitational Anti-Screening; Penner 2016a, 2016b, 2018) is one example of theories that involve fields of mass dipoles contributing to the gravitational field (Blanchet 2007a, 2007b, Blanchet and Le Tiec 2008, Hajdukovic 2011a, 2011b, 2020). In the case of Hajdukovic's dipole theory, it is found to disagree with observations taken within the solar system (Banik&Kroupa 2020). In the case of GRAS, which is in agreement with solar system measurements (Penner 2020), it is hypothesised that baryonic masses are surrounded by a sea of virtual mass dipoles analogous to quantum electrodynamic theory (QED), where charges are surrounded by a sea of virtual electric dipoles. In QED, the alignment of the virtual electric dipoles results in a screening effect that leads to the observed charge of a particle being less than its actual bare charge. In GRAS, the alignment of the virtual mass dipoles results in an anti-screening effect that leads to the observed mass of a galaxy being greater than its baryonic mass.

Both AQUAL and GRAS lead to excellent agreement with the BTFR and the RAR. However, although these MOND-type theories are in good agreement with observations on the galactic scale, they run into problems when applied to galaxy clusters (Sanders 2003, McGaugh 2015). Extrapolating these theories to clusters of galaxies leads to gravitational fields that are too weak to explain the hydrostatic equilibrium of the X-ray emitting intracluster gas. Significantly more baryonic mass is required for such MOND-type theories to explain the observations. This also applies when trying to explain the lensing results from the Bullet cluster. In general, it would appear that to explain such large-scale structures, MOND-type theories also require some form of dark matter, albeit less than without such theories. Also, although GRAS does not require a change to Newtonian gravitational theory or GR, AQUAL does. However, the BTFR and even the RAR are in the realm of extremely weak gravitational fields, and deviations from Newtonian theory are not expected until the gravitational field falls to less than approximately 10^{-10} m s^{-2}. The most distant spacecraft from Earth is Voyager 1, at a distance of 157 au from the Sun. At this distance the solar gravitational field is approximately 2.4 x 10^{-7} m s^{-2}, several orders

of magnitude greater than where deviations are expected.

Although conceptually AQUAL and GRAS are quite different, both AQUAL and GRAS lead to the same field equation as shown by Penner (2022). As such, the results of this manuscript apply equally to both these gravitational theories. As tests of such MOND-type theories, previous studies have looked at line-of-sight intervelocities of very wide binary stars. Using samples taken from the GAIA catalogue, Pittordis&Sutherland (2023) concluded that Newtonian gravitational theory provides a better fit. However, this requires an unseen third star for a significant proportion of the binaries to explain the long tail in the velocity difference distribution. Hernandez et al (2022), also using samples taken from the GAIA catalogue, conclude that Newtonian gravity fails, and MOND-type gravity works better. Although the external field effect due to the Galaxy, which is found in MOND, should make the deviations from Newtonian theory less than what was found. Overall, these studies of wide binary stars are inconclusive.

In this manuscript, these theories of AQUAL and GRAS will be applied instead to isolated galaxy pairs. The analysis of binary galaxies would seem to be an excellent way of testing gravitational theories and determining whether the dynamics of binary galaxies can be explained by MOND-type theories. Unlike with binary stars within the Galaxy, the external field effect can be neglected, i.e., the effect of the gravitational field due to other distant galaxies. Being able to neglect external field effects leads to significantly greater deviations from Newtonian theory. The analysis of binary galaxies does however suffer from two major complications. First, as with binary stars, observations of binary galaxies only provide v_{los}, their line-of-sight intervelocities, r_p, their projected separations, and their luminosities. Combined with this limitation, the uncertainties and resulting scatter in datasets are typically large. The second complication is selecting a representative set of isolated pairs. The primary criteria for selecting binary galaxies in the various studies are their isolation and their relative velocities, but one is bound to have some optical pairs (chance alignments) included in the set. Also, one needs to be careful as such selection criteria may bias the results.

There have been several previous studies that have looked at the dynamics of binary galaxies (Turner 1976a, 1976b, Turner & Ostriker 1977, Peterson 1979a, 1979b, White 1981, Van Moorsel 1982, 1983a, 1983b, 1983c, 1987, White et al 1983, Schweizer 1987a, 1987b, Chengalur et al 1993, Honma 1999). These studies looked for relationships among the

observables, v_{los}, r_p, and galaxy luminosities, and compared these results to various theoretical models. The models were all based on the concept of dark matter halos surrounding individual galaxies. It was taken that the dark matter halos do not interact, and that the galaxies can be treated as point masses executing Keplerian orbits. A summary of the major conclusions reached by the different researchers is provided in Penner (2017). Several of the researchers concluded that the interaction between the pairs corresponds best to a logarithmic interaction potential (White 1981, White et al 1983, Van Moorsel 1982, 1983a, 1983b, 1983c, 1987). This is what would be expected if the observed relationships for spiral galaxies, i.e. the BTFR and RAR, apply as a $g \propto 1/r$ leads to a logarithmic interaction potential. However, in general, there was no conclusive answer regarding the dynamics of binary galaxies except that the dark matter haloes must be extremely massive, with the total mass of the pair being much greater than the sum of the individually estimated galaxy masses. The problem is partially related to the complications mentioned above, but it is also due to the model being used. In the author's opinion, researchers were trying to fit the data with a flawed model based on galaxies having dark matter halos of set size executing Keplerian orbits.

These studies were reconsidered in the context of GRAS (Penner 2017). The combined total of 208 binaries from these different studies were used, but in this case the relationship between v_{los} and the rotational velocities of the galaxies was now considered. Specifically, the expected distribution of $\tilde{v}$ that falls out from GRAS was determined, where $\tilde{v} \equiv v_{los}/v_R$, with v_R being the rotational velocity of the larger of the two galaxies. Only the theoretical cases where the mass of the larger galaxy was much greater than the smaller galaxy or where the masses of the two galaxies were the same were considered in the analysis. Also, only the distributions for circular and radial orbits were determined. The theoretical distributions of $\tilde{v}$ were then compared to the distributions for the sets of binaries from the various studies. It was found that the different studies were now consistent with each other and agreed with the theoretical distribution of $\tilde{v}$ that falls out from GRAS. Further, it was found that the resulting distribution of $\tilde{v}$ was consistent with the binaries orbiting on near radial orbits. These results will of course also apply to AQUAL.

More recently, Nottale & Chamaraux (2020) performed a statistical deprojection (Nottale and Chamaraux 2018a) of the v_{los}'s of different subsets of the 13114 galaxy pairs in their Isolated Galaxy Pair Catalog (IGPC; Nottale & Chamaraux 2018b). The resulting probability distribution of the intervelocities was characterized by a peak at approximately 150 km s^{-1} for all the

subsamples, with a possible second peak at approximately 360 km s^{-1}. Scarpa et al (2022) repeated this analysis for a different subset taken from the IGPC and, similarly, found a peak at approximately 130 km s^{-1}. Using the B-band absolute magnitudes of the selected galaxies, the distribution of the total luminous mass for the set was calculated. The MOND intervelocity distribution expected for the calculated total mass distribution was then determined in the case of equal mass components executing circular motion. The resulting MOND distribution has a peak centred at approximately 140 km s^{-1}, in good agreement with the observations. However, Pawlowski et al (2022) also found a similar intervelocity peak when they performed simulations of binary galaxies with accompanying dark matter halos. Therefore, the intervelocity peak found with binary galaxies is not a conclusive test of MOND and dark matter.

This manuscript will go further than the distribution of the intervelocites. It will expand on the author's previous work (Penner 2017) with a subset of 3970 highly isolated binary galaxies chosen from the IGPC used in the analysis. This is a substantially larger data set than what was previously considered. This large data set will allow the testing of a theoretical relationship between $\overline{v_{los}}$ and v_M, a parameter which depends on the individual baryonic masses of the galaxies. In addition, the distribution of $\tilde{v} \equiv v_{los}/v_M$ will be determined and compared to theory. Then following in the footsteps of Nottale & Chamaraux (2020) and Scarpa et al (2022), the probability distribution of the intervelocities will also be determined from the v_{los} of the subset. These results will then be compared to theoretical expressions derived for both circular and radial orbits.

2 AQUAL AND GRAS FIELD EQUATIONS

In Newtonian gravitational theory, the Langrangian is given by

$$\mathcal{L} = \frac{1}{8\pi G}|\nabla\Phi_N|^2 + \rho_b\Phi_N \,, \tag{8}$$

where Φ_N is the Newtonian gravitational scalar potential and ρ_b is the baryonic mass density. Solving the Lagrange equation then leads to the Newtonian field equation

$$\nabla \cdot \nabla\Phi_N = 4\pi G\rho_b. \tag{9}$$

In the AQUAL gravitational theory, the non-relativistic Lagrangian is given by

$$\mathcal{L} = \frac{1}{8\pi G} g_o^2 \, F\left(\frac{|\nabla\Phi|^2}{g_o^2}\right) + \rho_b\Phi \,, \tag{10}$$

with F being an arbitrary function and g_o being a parameter that is to be determined by observations. In the case of spherical symmetry, this Lagrangian leads to the following modified Newtonian field equation

$$\boldsymbol{\nabla} \cdot (\mu(|\boldsymbol{\nabla}\Phi|/g_o)\boldsymbol{\nabla}\Phi) = 4\pi G\rho_b \,, \tag{11}$$

or equivalently by (9) and (11)

$$\mu(g/g_o)\mathbf{g} = \mathbf{g_N}, \tag{12}$$

with $\mathbf{g} = \boldsymbol{\nabla}\Phi$ and $\mathbf{g_N} = \boldsymbol{\nabla}\Phi_N$. The function $\mu(g/g_o)$, referred to as the interpolating function, therefore determines the deviation between the AQUAL and Newtonian gravitational fields. The function μ is related to the function F in (10) by

$$\mu(x) = \frac{dF(v)}{dv}\,, \tag{13}$$

with $x \equiv g/g_o$ and $v \equiv x^2$. To have agreement with both Newtonian theory within the solar system (Hees et al 2014, Hees et al 2016) and the BTFR, the interpolating function must be such that

$$\mu(g/g_o) \to 1 \qquad \text{for } g >> g_o, \tag{14a}$$

and

$$\mu(g/g_o) \to \frac{g}{g_o} \qquad \text{for } g << g_o. \tag{14b}$$

For $g << g_o$, by (12) and (14b) the relationship between the Newtonian gravitational field g_N and the AQUAL gravitational field g is then

$$g = (g_N g_o)^{1/2}, \tag{15}$$

which leads to the BTFR.

Following in the steps of AQUAL, a non-relativistic Lagrangian for the GRAS gravitational theory can be expressed as

$$\mathcal{L} = \frac{1}{8\pi G}|\boldsymbol{\nabla}\Phi|^2 + \rho_b\Phi - \frac{1}{8\pi G}g_o^2\, K\left(\frac{|\boldsymbol{\nabla}\Phi|^2}{g_o^2}\right)\,, \tag{16}$$

where K is an arbitrary function. This Lagrangian leads to the following field equation

$$\boldsymbol{\nabla}\cdot\boldsymbol{\nabla}\boldsymbol{\Phi} = 4\pi G\rho_b + \boldsymbol{\nabla}\cdot(f(|\boldsymbol{\nabla}\Phi|/g_o)\boldsymbol{\nabla}\Phi)\,, \tag{17}$$

or equivalently by (9) and (17)

$$\big(1 - f(g/g_o)\big)\mathbf{g} = \mathbf{g_N}\,, \tag{18}$$

where the function f is related to the function K in (16) by

$$f(x) = \frac{dK(v)}{dv}\,. \tag{19}$$

The Lagrangian and field equation for GRAS are fundamentally the same as for AQUAL, with the two arbitrary functions related by K=v-F and the interpolating functions related by $f(g/g_o)$=1-$\mu(g/g_o)$. By (14), the subsequent conditions on the function $f(g/g_o)$ are

$$f(g/g_o) \rightarrow 0 \qquad \text{for } g >> g_o, \tag{20a}$$

and

$$f(g/g_o) \rightarrow 1 - \frac{g}{g_o} \qquad \text{for } g << g_o. \tag{20b}$$

Just as with AQUAL, these conditions lead to agreement with observations within the solar system (Hees et al 2014, Aurelien et al 2016) and with the BTFR.

With respect to the RAR, consider the following interpolating function which satisfies (20):

$$f(g/g_o) = \left(1 + \frac{g}{2g_o}\right)^{-2}, \tag{21}$$

with the corresponding function K(v) given by

$$K(v) = 8\ln\left(\sqrt{v} + 2\right) + \frac{16}{\sqrt{v}+2}\,. \tag{22}$$

A comparison between (18), using (21), and the RAR is shown in Figure 1. As is seen, using (21) for the interpolation function gives slightly lower values for g than the RAR, but overall the agreement is good.

Conceptually, the AQUAL field equation, (11), is taken to be a modification of current gravitational theory but with the same gravitational source, ρ_b, as with Newtonian theory. In GRAS, Newtonian gravitational theory holds, but there is an additional contribution to the gravitational field from a sea of virtual mass dipoles surrounding a given baryonic mass. This can be shown as follows.

Analogous to electromagnetic theory, the equivalent mass density ρ_d for a field of mass dipoles is given by

$$\rho_d = -\nabla \cdot \mathbf{P}\,, \tag{23}$$

where **P** is the mass dipole moment density. The dependence that **P** has on the total gravitational field **g** can be expressed as

$$\mathbf{P} = \frac{1}{4\pi G}\, f(g/g_o)\mathbf{g}\,, \tag{24}$$

with the function $f(g/g_o)$ incorporating any nonlinearity between **P** and **g**. The field equation for GRAS, equation (17), can then be expressed as

$$\boldsymbol{\nabla} \cdot \boldsymbol{\nabla}\Phi = 4\pi G(\rho_b + \rho_d)\,. \tag{25}$$

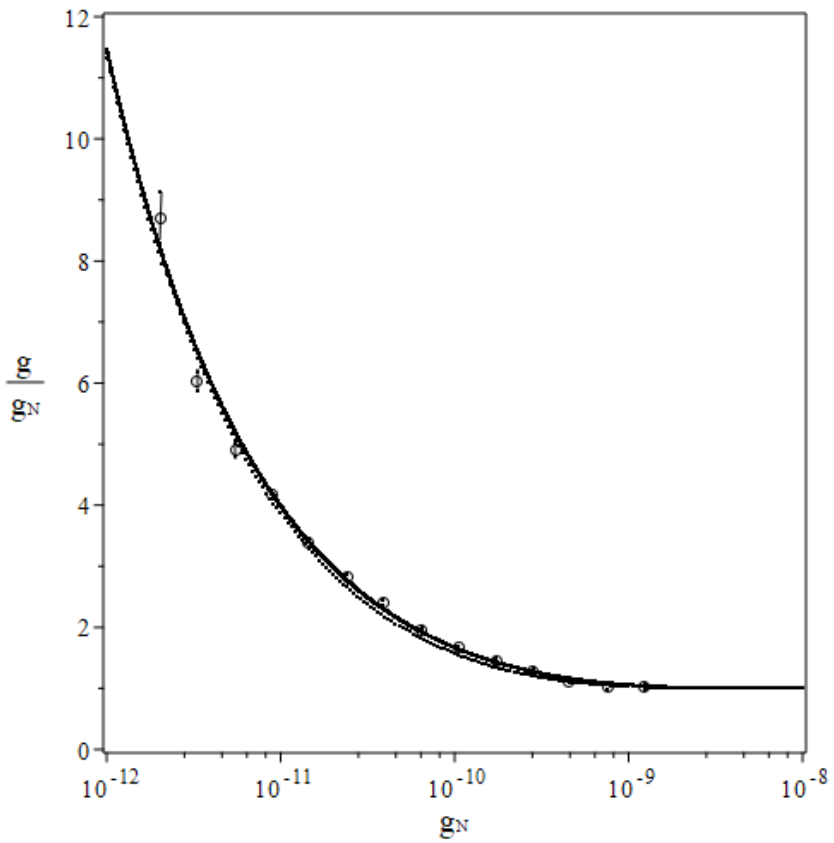

Figure 1: The ratio of g to g_N for both the RAR, i.e. (2), (solid line), and GRAS/AQUAL, i.e. (18) using the interpolating function given by (21), (····). Included on the figure are the mean bin values along with their 1σ uncertainties for the data points used in generating the RAR (McGaugh et al 2016).

3 APPLICATION TO BINARY SYSTEMS

3.1 Determination of relative acceleration

For both AQUAL or GRAS, the field equation can be expressed as (25) either with

$$\rho_d = \frac{1}{4\pi G}\nabla \cdot (f(g/g_o)\nabla\Phi) \,, \tag{26}$$

for GRAS, or

$$\rho_d = \frac{1}{4\pi G}\nabla \cdot ((1-\mu(g/g_o))\nabla\Phi) \,, \tag{27}$$

for AQUAL. In the case of AQUAL, ρ_d is taken to be a phantom density, a tool used to assist in solving the field equation. In GRAS, ρ_d is a real mass density due to a field of virtual dipoles. In either case, a technique for solving the nonlinear field equation is as follows. The initial estimate of Φ is taken to be equal to Φ_N, i.e., that solely due to the baryonic masses of the two galaxies. Then (26), with an interpolating function *f* such as given by (21), is solved for an initial estimate

of the distribution of ρ_d. For the next estimate, the total Φ is then taken to be equal to the sum of that due to the baryonic masses and that due to the estimate of ρ_d. This iterative process is repeated until the resulting values of the total gravitational field obtained after a given iteration vary by less than a set amount from the previous iteration.

As an example, Figure 2 shows the resulting theoretical distribution of ρ_d, using (21), around pairs of galaxies with different baryonic masses. In the figure, the two galaxies are separated by s = 100 kpc which is assumed to be great enough that their baryonic distributions can be treated as point masses. In general, the distribution of ρ_d associated with a particular galaxy or with a given pair does not terminate as with dark matter halos, but will extend out to the point where the gravitational field from the given baryonic mass distribution stops becoming dominant due to external fields from other structures. As is seen in the figures, the distribution due to ρ_d tends towards spherical symmetry at great enough distances, where the pair of galaxies then behave as a single mass.

From the distribution of ρ_d around the two galaxies, the gravitational acceleration of each galaxy, and thereby the relative acceleration of the two, can be determined for given separations. In general, this would be quite computationally intensive as the two galaxies affect each others distribution of ρ_d, as is seen in Figure 2, and this effect will depend on their separation. For our purposes though, the separation will in general be great enough that the two galaxies can be treated as point masses and $g << g_o$. In this case, an analytical expression for the relative acceleration between the two masses has been determined. This is given by (Milgrom 1994, Zhao et al. 2010)

$$a_{rel} = \frac{Q\sqrt{GM_{bary}g_o}}{r}, \tag{28a}$$

with

$$Q = \frac{2\left(1-q_1^{\frac{3}{2}}-q_2^{\frac{3}{2}}\right)}{3q_1q_2}, \tag{28b}$$

where M_{bary} is the total baryonic mass, $q_1 = M_1/M_{bary}$, and $q_2 = M_2/M_{bary}$. Defining the velocity parameter

$$v_M = \left(Q\sqrt{GM_{bary}g_o}\right)^{1/2}, \tag{29}$$

the relative acceleration can be expressed by

$$a_{rel} = \frac{v_M{}^2}{r} . \qquad (30)$$

The value of g_o in (29) was given in (3).

The parameter v_M depends only on the baryonic masses of the two galaxies and the value of g_o. As seen with (30), a_{rel} depends inversely on the separation of the two galaxies. A complication for the analysis of such an acceleration is that it does not lead to closed orbits. Therefore, only the two special cases that do lead to closed orbits will be considered, namely circular orbits and purely radial orbits.

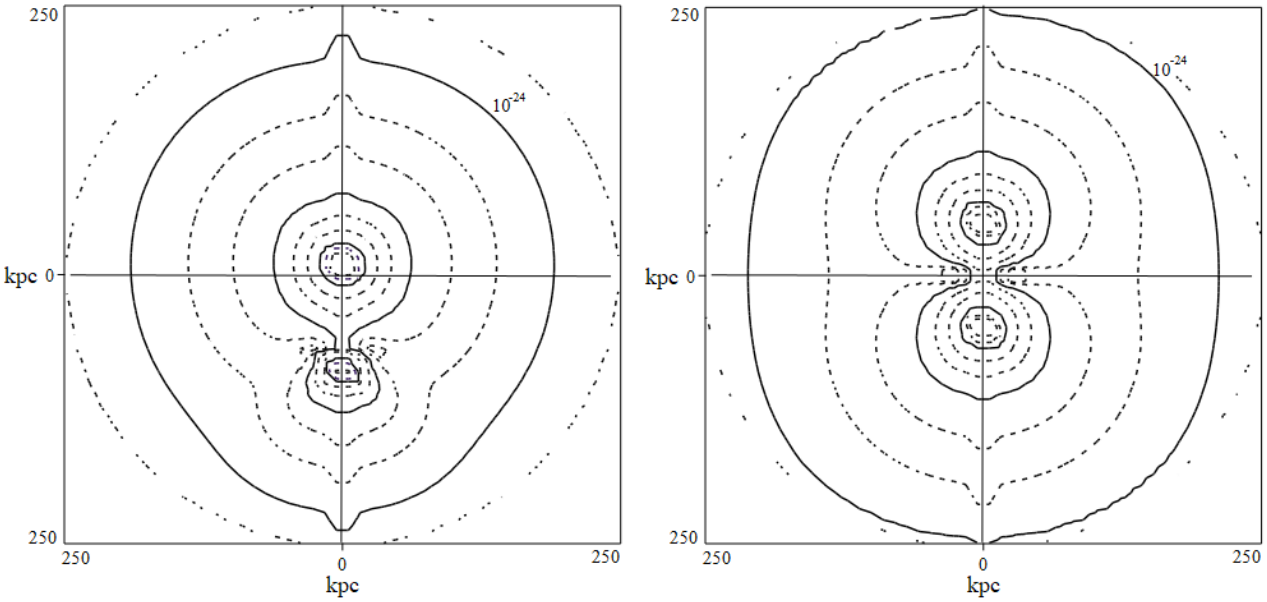

a) b)

Figure 2: The induced mass distribution ρ_d around a pair of galaxies separated by s = 100 kpc with $M_1 = 60 \times 10^9$ $M_\odot$ and (a) $M_2 = 6 \times 10^9$ $M_\odot$, (b) $M_2 = 60 \times 10^9$ $M_\odot$. The induced mass density lines shown are at values of 10^{-24} kg m^{-3}, 2×10^{-24} kg m^{-3}, 4×10^{-24} kg m^{-3}, 10^{-23} kg m^{-3}, 2×10^{-23} kg m^{-3}, 4×10^{-23} kg m^{-3}, and 10^{-22} kg m^{-3} as one moves from the outer solid line to the inner solid lines. The secondary bumps along the vertical axis are not real but are computational artifacts.

3.2.1 Circular orbits

In the case of circular orbits, the relative acceleration between the two masses is given by

$$a_{rel} = \frac{(v_1+v_2)^2}{r} , \qquad (31)$$

where v_1 and v_2 are the orbital speeds of the two galaxies. Comparing (30) and (31) it is seen that the relative velocity between the two galaxies, $v_{rel} = v_1 + v_2$, is simply given by

$$v_{rel} = v_M. \quad (32)$$

As is seen with (29) and (32), with MOND-type theories the relative velocity is independent of the separation of the two galaxies. As discussed in the introduction, observations of binary galaxies do not directly provide v_{rel} but provide v_{los}, the line-of-sight velocity difference between their galactic centres. However, a relationship between $\overline{v_{los}}$ and v_{rel} can be determined. First, for an angle θ between $\mathbf{v_{rel}}$ and the line-of-sight from the Earth, it follows that

$$v_{los} = v_{rel} \cos\theta. \quad (33)$$

If there is no preferred direction for $\mathbf{v_{rel}}$, so that in a representative set of binary galaxies the $\mathbf{v_{rel}}$'s are equally distributed in all directions, the probability function for θ will be given by

$$P(\theta) = \sin\theta \qquad 0 < \theta < \pi/2\ . \quad (34)$$

The probability function for the line-of-sight velocity $P(v_{los}|v_{rel})$, for a given v_{rel}, is in turn determined by

$$P(v_{los}|v_{rel})dv_{los} = -P(\theta)\ d\theta\ , \quad (35)$$

which leads to

$$P(v_{los}|v_{rel}) = P(\theta)\left(\frac{-\,dv_{los}}{d\theta}\right)^{-1}. \quad (36)$$

By (33), (34), and (36),

$$P(v_{los}|v_{rel}) = \frac{1}{v_{rel}} \quad 0 \le v_{los} \le v_{rel}\ , \quad (37)$$

and therefore, for any v_{rel}, v_{los} is uniformly distributed over the range 0 to v_{rel}. The average line-of-sight velocity for a given v_{rel} is then given by

$$\overline{v_{los}} = \int_0^{v_{rel}} v_{los} P(v_{los}|v_{rel}) dv_{los} \quad (38a)$$

$$= 0.50\ v_{rel}\ . \quad (38b)$$

Equations (37) and (38) are valid for both circular and radial orbits. In the specific case of circular orbits, (32) also applies. Therefore, in the case of circular orbits, for a set of binary galaxies which have the same baryonic masses, and thereby the same v_M,

$$P(v_{los}|v_M) = \frac{1}{v_M} \quad 0 \le v_{los} \le v_M, \quad (39a)$$

and

$$\overline{v_{los}} = 0.50\ v_M. \quad (39b)$$

We can also consider a set of binary galaxies which have different v_M's by defining

$$\tilde{v} \equiv v_{los}/v_M \, , \tag{40}$$

i.e., $\tilde{v}$ is equal to the ratio of the line-of-sight velocity difference of a pair of galaxies to their velocity parameter. The probability function for $\tilde{v}$ will be given by

$$P(\tilde{v}) = P(v_{los}|v_M) \, \frac{dv_{los}}{d\tilde{v}} \, . \tag{41}$$

By (39) and (40), (41) becomes

$$P(\tilde{v}) = 1 \qquad 0 \leq \tilde{v} \leq 1 \, . \tag{42}$$

with the average value of $\tilde{v}$ for circular orbits given by

$$\bar{\tilde{v}} = \int_0^1 \tilde{v} \, P(\tilde{v}) d\tilde{v} \, . \tag{43a}$$

$$= 0.50 \, . \tag{43b}$$

Equations (39), (42), and (43) represent the theoretical relationships for a set of binary galaxies that are on circular orbits.

3.3 Radial orbits

In the case of radial orbits, v_1, v_2, and the relative velocity, $v_{rel} = v_1 + v_2$, between the two galaxies will not be constant. For this case, the relative acceleration of the two galaxies will be given by

$$a_{rel} = \frac{dv_{rel}}{dt} = \frac{(v_M)^2}{r} \, . \tag{44}$$

Taking that apogee occurs at $r = r_o$, and integrating (44) results in

$$v_{rel} = \left(2 \ln\left(\frac{r_o}{r}\right)\right)^{1/2} v_M \, . \tag{45}$$

Integrating (45) then leads to the following dependence that r, the separation of the two galaxies, has on the time t,

$$r = r_o \, e^{-\left(erfinv\left(\frac{t}{\tau}\right)\right)^2} , \tag{46}$$

where *erfinv* is the inverse error function and τ, the time it takes to go from $r = r_o$ to $r = 0$, i.e., ¼ of a period, is given by

$$\tau = \left(\frac{\pi}{2}\right)^{1/2} \frac{r_o}{v_M} \, . \tag{47}$$

Equation (47) is the same for the case of a free-falling particle in the deep-MOND limit, except in that case v_M in (47) is set equal to v_f for the given galaxy (Banik&Zhao 2018).

To determine $P(v_{los}|v_M)$ in the case of radial orbits, (45) is first inverted, leading to

$$r = r_o\, e^{-\frac{1}{2}\left(\frac{v_{rel}}{v_M}\right)^2}. \tag{48}$$

The probability function for r can then be determined from

$$P(r)dr = -P(t)dt\,, \tag{49}$$

where it is taken that the galaxies are approaching each other, i.e., r is decreasing with t.

Given that

$$P(t) = 1/\tau \;\; 0 \le t \le \tau\,, \tag{50}$$

as all times are equally probable, (49) then becomes

$$P(r) = \frac{1}{\tau}\left(\frac{-dr}{dt}\right)^{-1} \tag{51a}$$

$$= \frac{1}{\tau\, v_{rel}}\,. \tag{51b}$$

The resulting probability function for v_{rel} is then determined by

$$P(v_{rel}|v_M)dv_{rel} = -P(r)\; dr\,, \tag{52}$$

leading to

$$P(v_{rel}|v_M) = P(r)\left(-\frac{dr}{dv_{rel}}\right). \tag{53}$$

By (48) and (51), (53) becomes

$$P(v_{rel}|v_M) = \frac{r_o}{\tau\,(v_M)^2}\; e^{-\frac{1}{2}\left(\frac{v_{rel}}{v_M}\right)^2}. \tag{54}$$

Substituting (47) into (54) then results in

$$P(v_{rel}|v_M) = \left(\frac{2}{\pi}\right)^{1/2}\frac{1}{v_M}\; e^{-\frac{1}{2}\left(\frac{v_{rel}}{v_M}\right)^2}. \tag{55}$$

If the probability function of v_M for a given set of isolated pairs is known, then the probability function for v_{rel}, in the case of radial orbits, will be given by

$$P(v_{rel}) = \int_0^\infty P(v_{rel}|v_M)\, P(v_M)dv_M\,, \tag{56}$$

with $P(v_{rel}|v_M)$ as given by (55).

In terms of v_{los}, by (37) and (55) it then follows that

$$P(v_{los}|v_M) = \int_{v_{los}}^\infty P(v_{los}|v_{rel})\, P(v_{rel}|v_M)dv_{rel} \tag{57a}$$

$$= \left(\frac{2}{\pi}\right)^{1/2} \frac{1}{v_M} \int_{v_{los}}^{\infty} \frac{1}{v_{rel}} e^{-\frac{1}{2}\left(\frac{v_{rel}}{v_M}\right)^2} dv_{rel} \quad (57b)$$

$$= -\left(\frac{1}{2\pi}\right)^{1/2} \frac{1}{v_M} \, \mathrm{Ei}\left(-\frac{1}{2}\left(\frac{v_{los}}{v_M}\right)^2\right), \quad (57c)$$

where Ei is the function known as the exponential integral.

As with circular orbits, we can consider a subset of binary galaxies which have the same v_M. In this case, the distribution as given by (57) leads to

$$\overline{v_{los}} = \int_0^{\infty} v_{los} P(v_{los}|v_M) dv_{los} \quad (58a)$$

$$= -\left(\frac{1}{2\pi}\right)^{1/2} \int_0^{\infty} \frac{v_{los}}{v_M} \, \mathrm{Ei}\left(-\frac{1}{2}\left(\frac{v_{los}}{v_M}\right)^2\right) dv_{los} \quad (58b)$$

$$= \left(\frac{1}{2\pi}\right)^{1/2} v_M \quad (58c)$$

$$\cong 0.40 \, v_M \, . \quad (58d)$$

By (41) and (57), the probability function for $\tilde{v}$ in the case of radial orbits is given by

$$P(\tilde{v}) = -\left(\frac{1}{2\pi}\right)^{1/2} \mathrm{Ei}\left(-\frac{\tilde{v}^2}{2}\right) \quad (59a)$$

$$= -0.40 \, \mathrm{Ei}\left(-\frac{\tilde{v}^2}{2}\right), \quad (59b)$$

with the average value of $\tilde{v}$ for radial orbits given by

$$\bar{\tilde{v}} = \int_0^{\infty} \tilde{v} \, P(\tilde{v}) d\tilde{v} \quad (60a)$$

$$= \left(\frac{1}{2\pi}\right)^{1/2} \quad (60b)$$

$$\cong 0.40 \, . \quad (60c)$$

This value is below the result for circular orbits, i.e. (43), because most of the time on a highly eccentric orbit is spent near apocentre, where the relative velocity is much smaller than the circular orbit velocity.

3.4 Predicted velocity relationships

By (39) and (58), it is predicted by AQUAL and GRAS that for a set of binary galaxies which have a given rotational parameter v_M, $\overline{v_{los}}$ is directly proportional to v_M with

$$\overline{v_{los}} \cong (0.40 \rightarrow 0.50) v_M \, . \quad (61)$$

In addition, for a set of binary galaxies with different v_M's, the expected probability functions for $\tilde{v}$ according to AQUAL and GRAS in the cases of circular and radial orbits are given by (42) and

(59), respectively. These two distributions are shown on Figure 3. These theoretical velocity relationships will now be compared with observations.

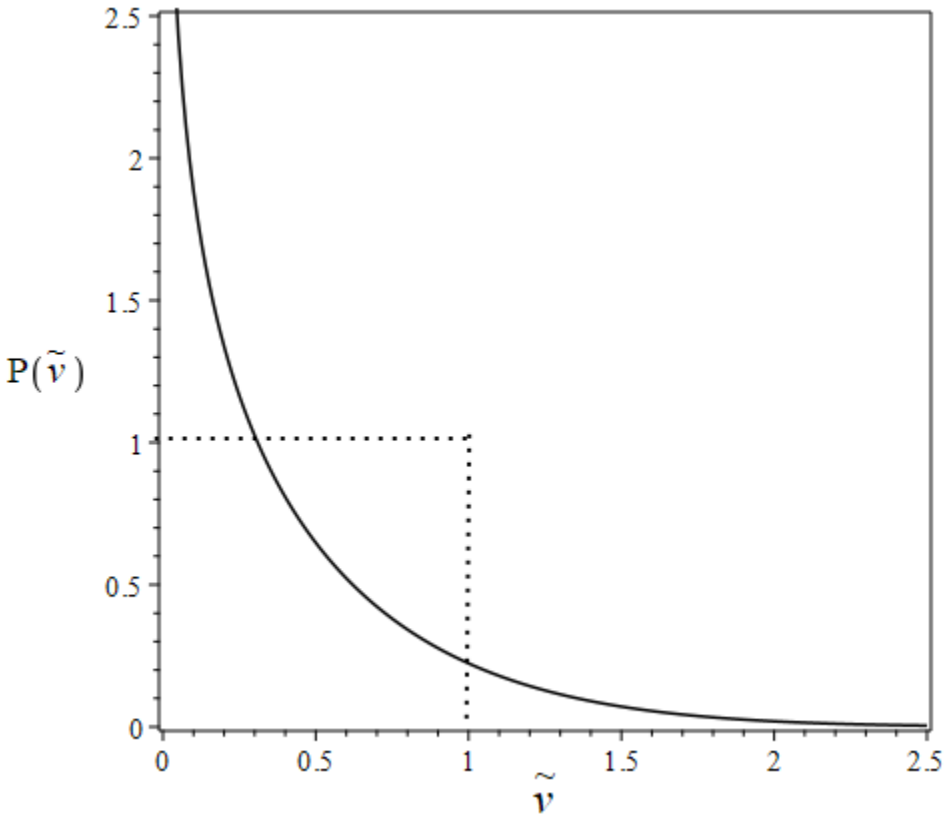

Figure 3: P(ṽ) for both circular (····) and radial (solid line) orbits.

4 RESULTS

4.1 Binary galaxy sample

The set of binary galaxies that will be considered come from the IGPC constructed by Nottale and Chamaraux (2018). The catalogue consists of 13114 pairs which have projected separations < 1 Mpc and radial velocity differences < 500 km/s. To ensure that the highest percentage of galaxy pairs used in the analysis are strict binaries and not part of a larger system, we will use the isolation criteria $\rho = r_3/r_p \geq 10$, where r_3 is the projected distance of the next nearest galaxy to the centre of the pair and r_p is the projected separation of the pair. This criterion reduces the number of pairs to 4268.

To compare the theoretical results with the data set values, the baryonic mass of each galaxy needs to be known. The data set provides the B-band luminosity for each galaxy, with an average magnitude of M_B = -20.0 and a range of $M_B \cong$ -18.5 → -22. In the B-band, expected stellar mass-to-light ratios are in the range of 1-2 (McGaugh&Blok 1998). Given the existence of gas within galaxies, the B-band total baryonic mass-to-light ratio will be higher than the stellar mass-to-light ratio. As such, for the purposes of this manuscript, we will take the B-band total baryonic mass-to-light ratios, M_*/L_*, to be equal to 2, with each galaxy converted to its estimated baryonic mass using this ratio.

In determining any further criteria to be used to select the set of binary galaxies, there is a trade off between the quality and quantity of data. The more pairs in a set the better the statistics, however it is crucial to remove as many false or optical binaries as possible. This is accomplished by reducing the maximum projected separation and/or reducing the maximum allowed v_{los}. The reduction of the maximum allowed projected separation to 0.5 Mpc reduces the number of qualified pairs by only 56, down to 4268. As such, the maximum projected separation was left at 1 Mpc.

The limit on v_{los} is more problematic. A limit of 500 km s^{-1} is very reasonable if Newtonian dynamics prevails or if the orbits under AQUAL or GRAS dynamics are circular. However, if the dynamics are as given by AQUAL or GRAS and the orbits are non-circular, intervelocities between larger galaxies can easily exceed 500 km/s. In addition, having such a limit will lead to a bias between smaller galaxy pairs and larger ones. For example, if v_M is 125 km/s then the limit of 500 km/s allows for $\tilde{v}$'s up to 4, while if v_M is 300 km/s, the limit allows for $\tilde{v}$'s of only up to 1.6. To treat all galaxy pairs equally the additional criteria that $\tilde{v} \leq 2$ and $v_M \leq 250$ km s^{-1} was applied. This reduced the number of pairs in the set from 4268 down to 3970. Of course, by limiting $\tilde{v}$ there will still be a bias towards certain orbits, but at least all pairs in the set are treated equally. For this data set the average projected separation is 90 kpc, with the maximum projected separation of 978 kpc. The distribution of projected separations is shown on Figure 4. The value of Q as given by (28b) for the data set does not vary much with the average value given by

$$\overline{Q} = 0.797 \pm 0.020 \,. \tag{62}$$

Given the limits on projected separations and velocity differences one does need to be careful with conclusions and not put too much weight on secondary effects. The primary goal

here is to determine if the theoretical predictions of AQUAL or GRAS with regards to the relationships between v_{los} and v_M, as given by (39), (42), (58), and (59), agree with the observations.

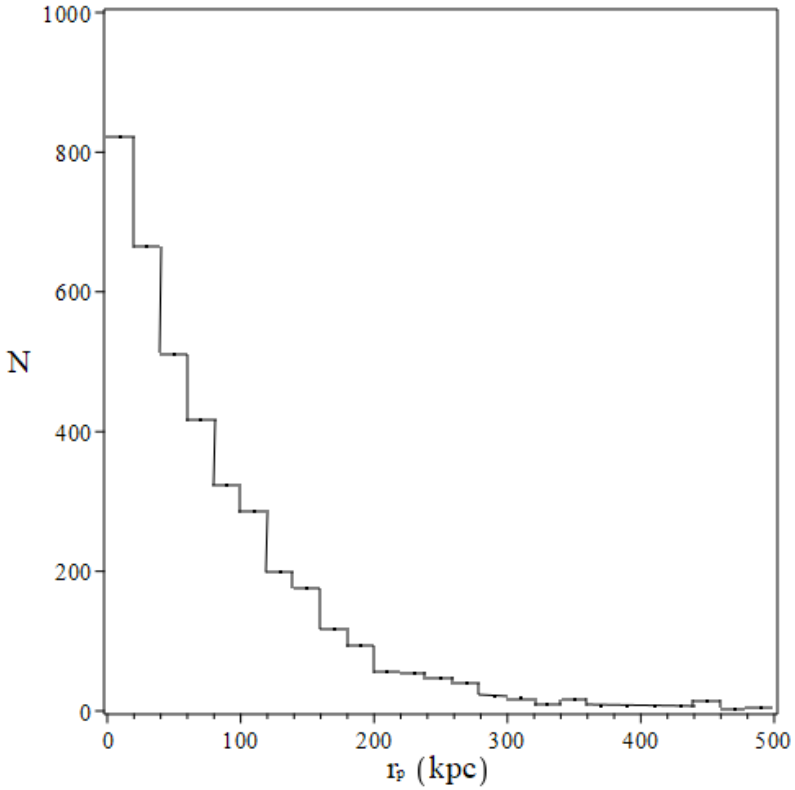

Figure 4: The distribution of projected separations for the 3918 binary galaxies which have $r_p \leq$ 500 kpc. The remaining 52 of the 3970 pairs have $r_p >$ 500 kpc and are not shown in the figure. The bin size is 20 kpc.

4.2 Observed velocity relationships

The velocity parameter v_M, as given by (29), was calculated for each of the binary pairs in the set. The binaries were then separated into 15 equal bins covering the range 100 to 250 km s^{-1}. Then $\overline{v_{los}}$ was calculated for each subset. The results are shown on Figure 5. As is seen in the figure, $\overline{v_{los}}$ is correlated to v_M, as predicted. The weighted best fit line, included on the figure, is given by

$$\overline{v_{los}} = (0.523 \pm 0.057)v_M + (19 \pm 10) \text{ km s}^{-1} . \quad (63)$$

The y-intercept, or offset, is what would be expected if false pairs were being included in the data set. For such pairs, $\overline{v_{los}}$ would be uniformly distributed, independent of v_M, leading to an additional constant added to all bins.

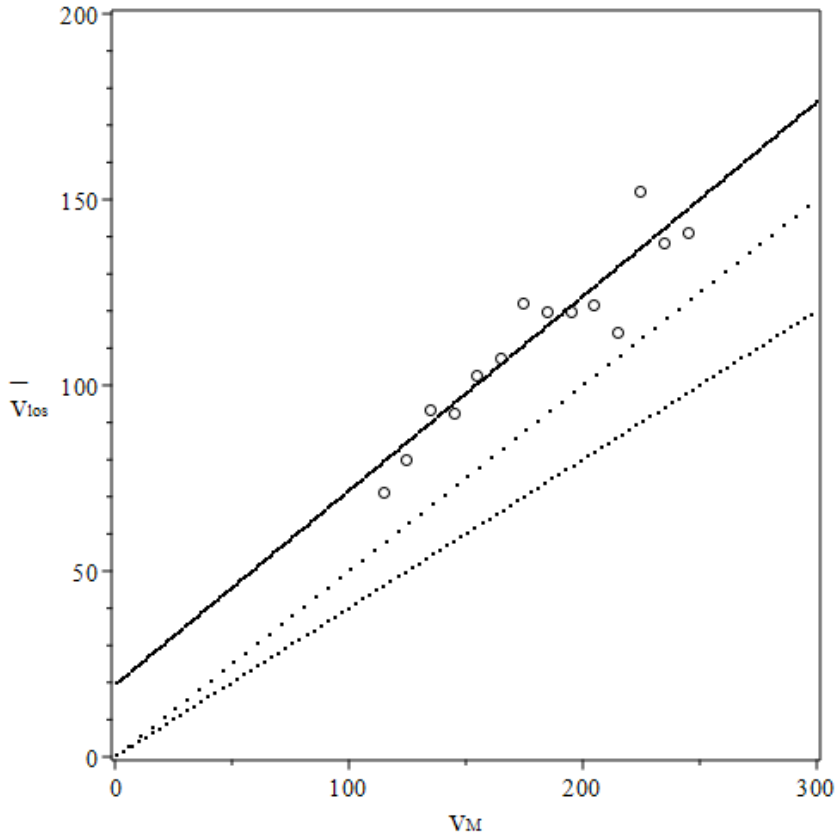

Figure 5: The data set with the best fit least squares line. Included are the predictions for radial orbits (···) and circular orbits (· · ·).

Also included on the figure are the predictions from AQUAL and GRAS, namely that the slope should lie between the values of 0.40 and 0.50. Although the observed slope is slightly higher than these values, overall, the agreement between the observation and the prediction is quite good. Using the slope from (63), along with the values for g_o and Q as given by (3) and (62), (29) leads to the following Baryonic Tully-Fisher type relationship for binary galaxies,

$$M_{bary} = A_{BG}\, \overline{v_{los}}^4 , \tag{64a}$$

where

$$A_{BG} = (1.32 \pm 0.58)\ \text{x}\ 10^3\ M_\odot\ \text{km}^{-4}\text{s}^4 . \tag{64b}$$

Just as with the regular BTFR for single galaxies, the velocity of interest just depends on the baryonic mass and not on distance.

The value given in (64b) differs from the BTFR and RAR values as given by (1b) and (7b) because of projection effects, orbital ellipticity, a geometric correction in the cases of the

BTFR and RAR, as well as the affect that each galaxy has on the others ρ_d distribution. To show this, consider the case of the binary galaxies being on circular orbits. In this case, $\overline{v_{los}} = 0.50\ v_{rel}$ and (64) becomes

$$M_{bary} = A_{BGC} v_{rel}^{\ 4} \tag{65a}$$

where

$$A_{BGC} = (83 \pm 36) M_\odot\ km^{-4} s^4\ . \tag{65b}$$

Including the same correction to (65) that the BTFR and RAR have due to measurements of rotation velocities being taken in the disc of the galaxies, then leads to

$$A_{BGC*} = \alpha^{-1} A_{BGC} \tag{66a}$$

$$= (63 \pm 27) M_\odot\ km^{-4} s^4\ . \tag{66b}$$

Of course, the binary galaxies will in general not be on circular orbits and we are ignoring some effects. However, the above derivation does show that the Baryonic Tully-Fisher type relationship for binary galaxies given by (64) is a modified version of the standard BTFR.

To determine the nature of the orbits, the individual values of $\tilde{v}$ for each of the 3970 binaries were determined. The resulting distribution $P(\tilde{v})$ is shown on Figure 6 along with the AQUAL and GRAS predicted distributions, as given by (42) and (59). The resulting $P(\tilde{v})$ shown in the figure, based on observations, is in line with the predicted $P(\tilde{v})$'s that fall out of AQUAL or GRAS. In this case, we can go further and state that, in general, the orbits of binaries are not circular and tend towards radial. This is especially so as optical binaries would be expected to lead to a uniform distribution for $\tilde{v}$ between 0 and 2. More importantly, the primary conclusion from this result is that the distribution is in line with what would be expected if the dynamics of binaries are as follows from AQUAL and GRAS. The value of $\bar{\tilde{v}}$ for the set of 3970 binaries is

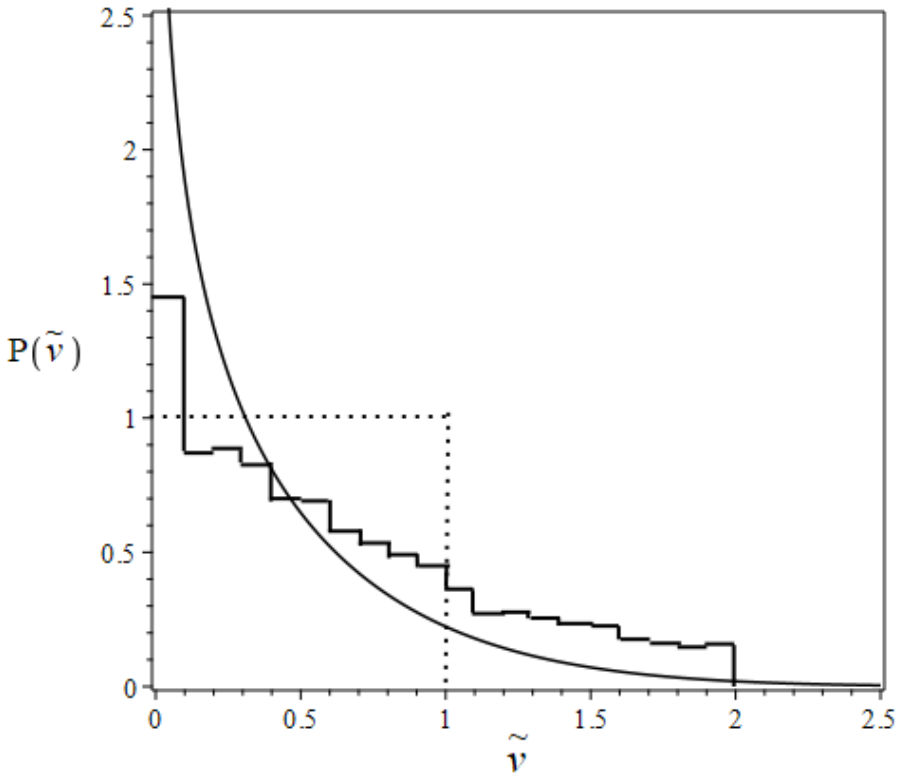

Figure 6: P(ṽ) for the 3970 binary galaxies in the data set, along with the theoretical distributions for circular (····) and radial (solid line) orbits.

found to be 0.65. As with the slope given in (63), this value is higher than the prediction of AQUAL and GRAS, which has a value between 0.40 and 0.50. This would be at least partly due to the optical binaries which would be expected to have a value of $\bar{\tilde{v}} = 1$, leading overall to a greater value for $\bar{\tilde{v}}$.

4.3 Determination of $P(v_{rel})$

To compare directly with the results of Nottale and Chamaraux (2018), the full set of 4268 highly isolated pairs, i.e. isolation criteria $\rho = r_3/r_p \geq 10$, will be used. Figure 7 shows the bin values for v_M for this given subset, with bin widths set to 10 km s^{-1}. Included in the figure are a pair of least squares best fit 3rd degree polynomials that were used in the analysis. The resulting probability function for v_M, $P(v_M)$, was then determined. In the case of circular orbits, by (32), $P(v_{rel}) = P(v_M)$. For radial orbits, $P(v_M)$ was inserted into (56) and $P(v_{rel})$ was determined. The resulting theoretical $P(v_{rel})$'s for the two cases, are shown in Figure 8.

The observational probability function for v_{rel} can be obtained directly from the probability function for v_{los} by using the following deprojection equation (Nottale & Chamaraux 2018a)

$$P(v_{rel}) = - v_{rel} \frac{dP(v_{los})}{dv_{los}} \Big|_{v_{los} = v_D} \quad (67)$$

In practice, using (67) is problematic as $P(v_{los})$ needs to be a monotonically decreasing function. To ensure such behaviour with real observational data, which will have statistical fluctuations, relatively large bin sizes are required. In line with the bin sizes used by Nottale and Chamaraux (2020), Figure 9 shows $P(v_{los})$ for the 4268 pairs with the bin size set at 30 km s^{-1}. Included on the figure is the following least squares best fitting 4th order polynomial,

$$P(v_{los}) = 0.0066065 - 0.000038816\, v_{los} + 9.318x10^{-8}\, {v_{los}}^2 - 1.060x10^{-10}\, {v_{los}}^3 + 4.744x10^{-14} {v_{los}}^4 \ , \quad (68)$$

where v_{los} is in km s^{-1}. The initial bin value, for 0 – 30 km s^{-1}, was not used in this fit as it was found to be problematic.

Substituting (68) into (67) then provides the expected $P(v_{rel})$ for the subset. The result is shown on Figure 10 along with Nottale & Chamaraux's results. Nottale & Chamaraux used differences in the bin values directly to calculate $P(v_{rel})$ from (67). As is seen in the figure, using the bin values directly leads to two peaks at approximately 150 km s^{-1} and 350 km s^{-1}, as they indicated in their paper. However, I believe that these are secondary features. The key feature is as shown using the fitted line, namely a broad peak centred at approximately 150 km s^{-1}. A benefit of fitting a line to $P(v_{los})$ is that this result is independent of bin size. Finally Figure 11 shows the $P(v_{rel})$, determined from $P(v_{los})$, along with the theoretical $P(v_{rel})$'s for circular and radial orbits. As is seen, the $P(v_{rel})$ for the 4268 pairs falls somewhere in between the two theoretical distributions. This hints at isotropic orbits leaning towards radial orbits. Overall, these results certainly lend support to GRAS and AQUAL or other MOND-like theories.

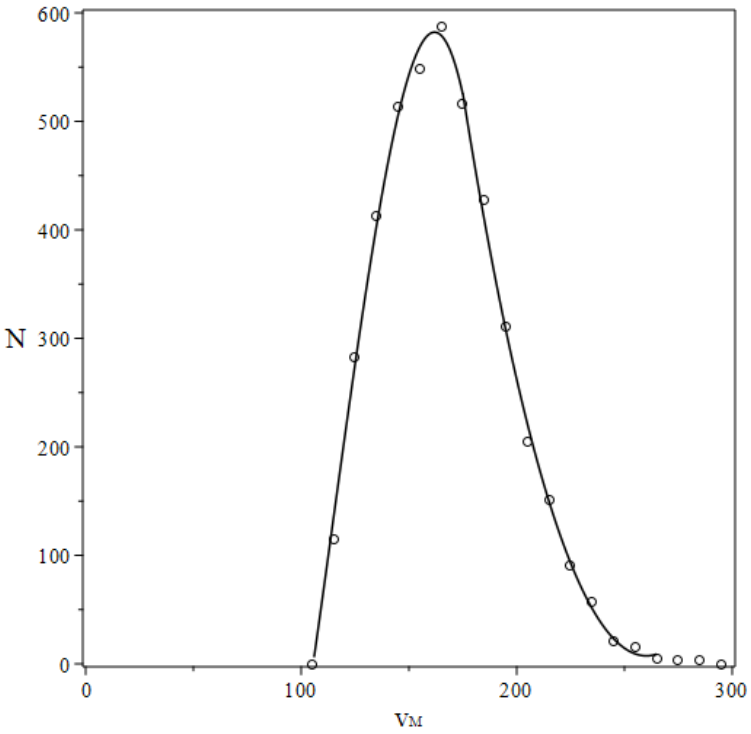

Figure 7: The bin values for v_M for the set of 4268 highly isolated pairs, with bin widths set to 10 km s^{-1}. The solid line is a pair of least squares best fit 3rd degree polynomials.

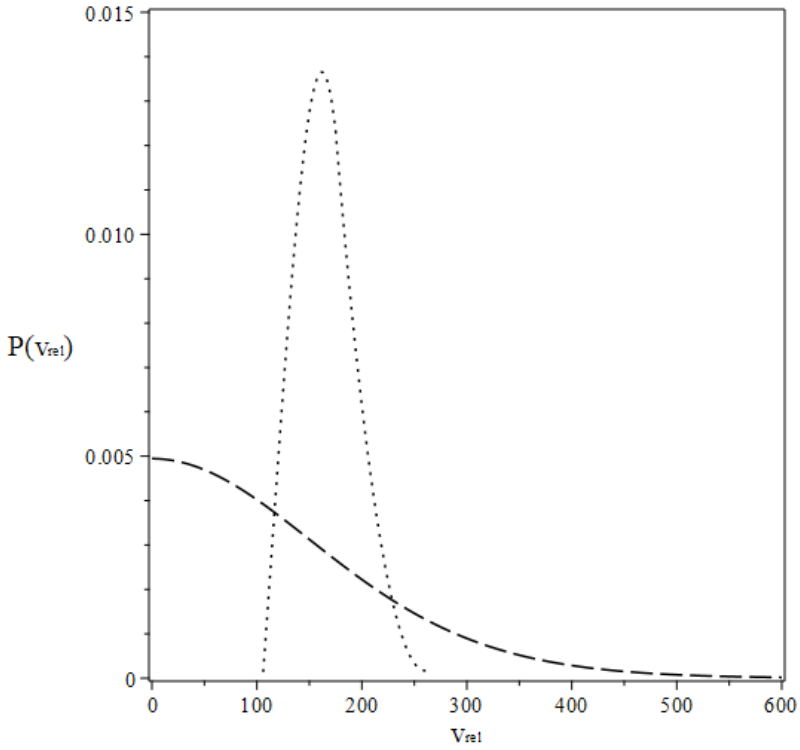

Figure 8: The theoretical $P(v_{rel})$'s in the cases of circular (····) and radial (----) orbits.

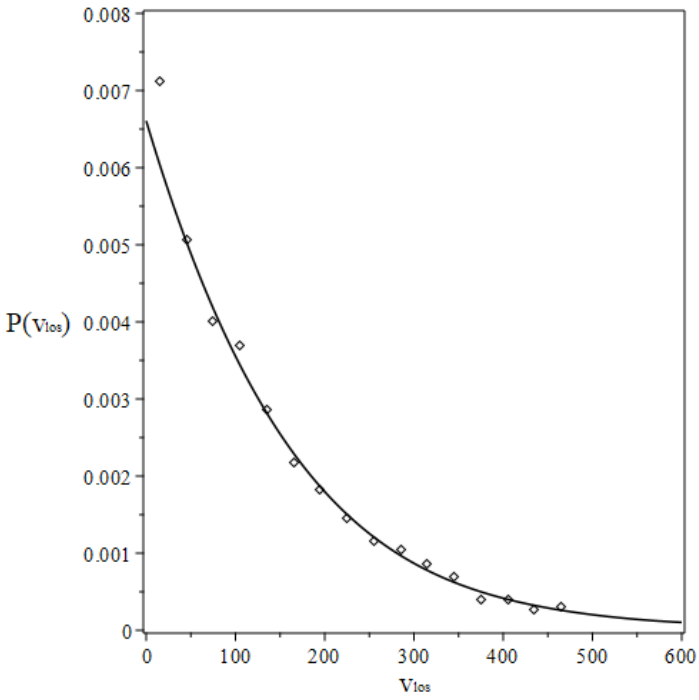

Figure 9: The bin values for $P(v_{los})$ for the 4268 pairs with the bin size set at 30 km s^{-1}. The solid line is the least squares best fitting 4th order polynomial, neglecting the first bin value.

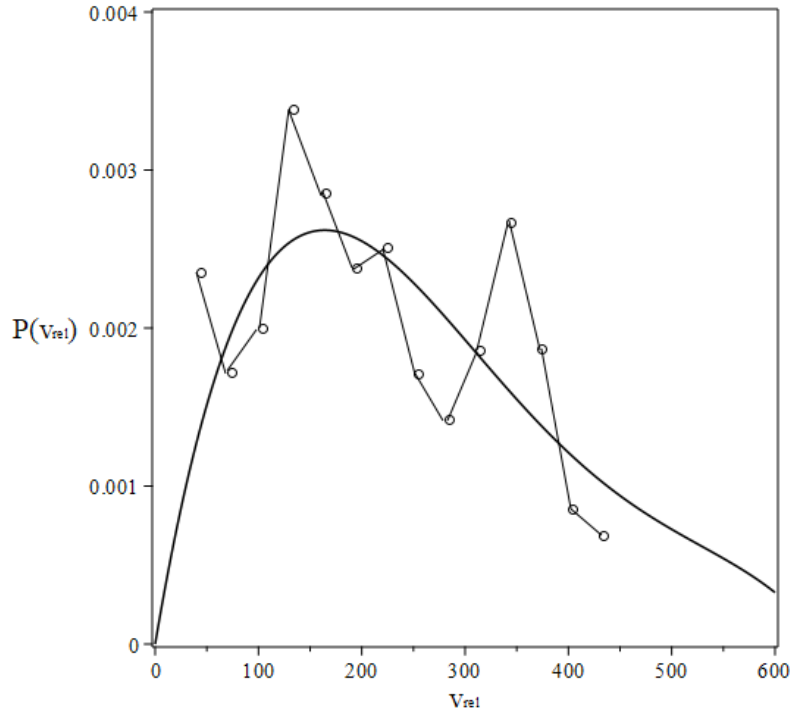

Figure 10: The resulting $P(v_{rel})$ obtained by deprojecting $P(v_{los})$. Values based on directly using bin values in the deprojection, as per Notalle & Chamaraux's, and the result based on the best fit line to $P(v_{los})$.

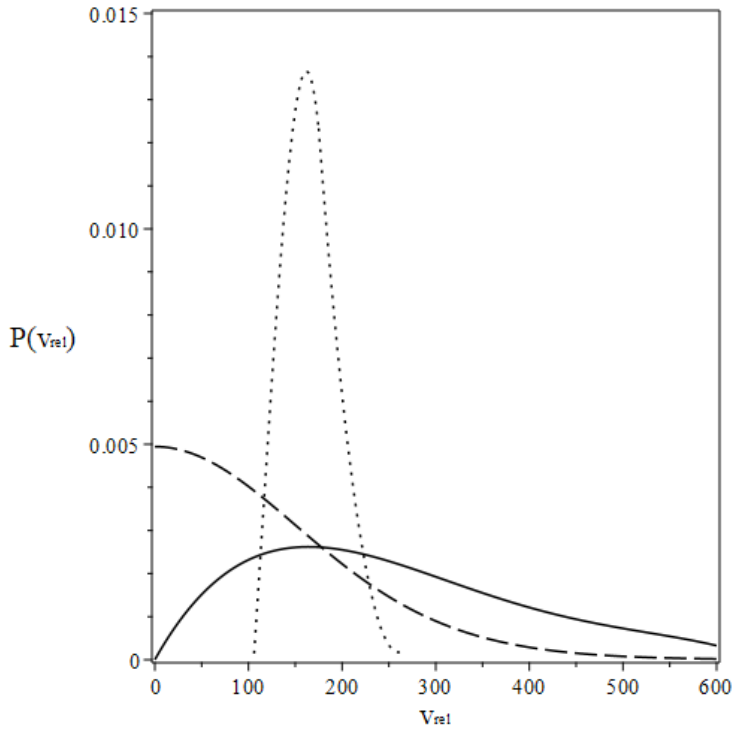

Figure 11: The resulting $P(v_{rel})$, obtained by deprojecting $P(v_{los})$, (solid line) along with the theoretical $P(v_{rel})$'s for circular (⋯) and radial orbits (----).

5 CONCLUSION

The primary goal of this manuscript was to determine whether the MOND-type theories of AQUAL and GRAS agree with observations of binary galaxies. It was found that the theoretical velocity relationships and distributions provided by AQUAL and GRAS are in good agreement with observations of a set of highly isolated pairs taken from the IGPC. Further, a Baryonic Tully-Fisher type relationship for binary galaxies was found. The agreement found between the modeled dynamics and observations of binary galaxies indirectly implies that there is no fall off in the rotational curves of galaxies, with the BTFR and RAR extending outward as far as the gravitational field of the galaxy dominates. Given that the average projected separations of galaxy pairs in the data set is 90 kpc with a maximum projected separation of 978 kpc, this is a significant extension of the BTFR and in turn the RAR. This result agrees with observational studies of galaxy groups, which are at the same distance scales (Banik&Zhao 2022). This also agrees with the results of Brouwer et al (2021) who used stacked weak lensing measurements on isolated galaxies to extend the RAR to values of $g_N < 10^{-14}$ m s^{-2}, at distances > 1 Mpc from the galaxies.

Given the scatter, the unbound pairs present in the set, and assumptions made with the theoretical model, it is somewhat risky to make secondary conclusions. However, the distributions of both $\tilde{v}$ and v_{rel} are indicative of orbits that tend towards radial. Further work will be needed to bring isotropic orbits into the picture. Another, more speculative secondary conclusion, relates to the values of both the slope of the v_{los} vs v_M best fit line and $\bar{\tilde{v}}$ being higher than the predicted values. If these are real effects and not related to the above points, it would indicate that the baryonic mass is significantly greater than what was estimated from the B-band magnitudes or that the MOND-type theories considered need to be modified at these larger distance scales. Speculating further, this may be related to the tension such MOND-type theories have with galaxy clusters which are at the same distance scales.

There was no attempt to consider the dynamics of binaries in the context of the theory of dark matter. As discussed in the introduction, previous researchers did so and their results indicate, to all intents and purposes, that the theory of dark matter struggles when applied to binary galaxies, even considering the results of Pawlowski et al (2022). This is not surprising given that the dark matter theory does not naturally lead to the BTFR and the RAR (Desmond 2017a,b).

Independently of the agreement with AQUAL and GRAS or any MOND-like theory, the results shown on Figures 5, 6, and 11 need an explanation. As with the BTFR and the RAR, these observations cannot be ignored.

ACKNOWLEDGEMENTS

I would like to thank the reviewer for very useful comments.

DATA AVAILABILITY:

No new data were generated or analysed in support of this research.

REFERENCES

Angus, G.W., Shan, Y.S., Zhao, H.S., Famaey, B., 2007, Astrophys. J., 654, L13

Aurelien H., Benoit F., Angus G.W., Gentile G., 2016, MNRAS, 455-1, 449

Banik I. & Zhao H., 2018, MNRAS, 473, 4033

Banik I. & Zhao H., 2022, Symmetry, 14- 7, 1331

Banik I. & Kroupa P., 2020, MNRAS, 495-4, 3974

Bekenstein J.D. & Milgrom M., 1984, ApJ, 286, 7

Blanchet L., 2007a, Class. Quant. Grav., 24, 3529, astro-ph/0605637

Blanchet L. 2007b, Class. Quant. Grav., 24, 3541, gr-qc/0609121

Blanchet L. & LeTiec A., 2008, arXiv.org/abs/0804.3518

Brouwer M.M., Oman K.A., Valentijn E.A., Bilicki M., Heymans C., et al., 2021, arXiv :2106.11677v1

Chae, K.H., 2022, Astrophys. J., 941 :55

Chengalur J.N., Salpeter E.E., Terzian Y., 1993, Astrophys. J., 419, 30

Desmond H., 2017a, MNRAS, 464-4, 4160

Desmond, H. 2017b, MNRAS, 472-1, L35

Famaey B. & McGaugh S., 2012, Living Reviews in Relativity, 15, 10

Hajdukovic D.S., 2011a, Astrophys. Space Sci., 334, 215

Hajdukovic D.S., 2011b, Adv. Astron., 196, 852

Hajdukovic D.S., 2020, MNRAS, 491-4, 4816

Hees A., Folkner W. M., Jacobson R. A., Park R. S., 2014, Phys. Rev. D, 89, 102002

Hees A., Famaey B., Angus G.W., Gentile G., 2016, MNRAS, 455, 449

Hernandez, X., Cookson S., Cortés R.A.M., 2022, MNRAS 509-2, 2304

Honma M., Astrophys. 1999, J., 516, 693

Kroupa P., 2014, Can. J. Phys., 93-2

Lelli F., McGaugh S.S., Schombert J.M., Pawlowski M.S., 2017, ApJ, 836-2, 152

McGaugh S.S., de Blok W.J.G., 1998, arXiv:Astro-ph/9801102v1

McGaugh S.S., Lelli F., & Schombert J.M., 2016, Phys. Rev. Lett., 117, 201101

McGaugh S. S., Schombert J. M., Bothun G. D., de Blok W. J. G., 2000, Astrophysical Journal Letters, 533-2, L99

McGaugh S.S., 2012, Astron. J, 143, 40

McGaugh S.S., 2015, Can. J. Phys., 93(2), 250

Milgrom M., 1983a, ApJ, 270, 365

Milgrom M., 1983b, ApJ, 270, 371

Milgrom M., 1983c, ApJ, 270, 384

Milgrom M., 1994, ApJ, 540

Navarro J.F., Frenk C.S., White S.D.M., 1996, ApJ, 462, 563

Navarro J.F., Frenk C.S., White S.D.M., 1997, ApJ, 490, 493

Nottale L., Chamaraux P., 2018a, Astron. Astrophys., 614, A45

Nottale L., Chamaraux P., 2018b, Astrophysical Bulletin, 73-3, 310

Nottale L., Chamaraux P., 2020, arXiv :2003.05940v1

Pawlowski M.S., 2021, Nature Astronomy, 5, 1185

Pawlowski M.S., Kanehisa K.J., Taibi S., Li P., 2022, A&A, 664, L6

Penner A.R., 2016a, Astrophys. Space Sci., 361, 124

Penner A.R., 2016b, Astrophys. Space Sci., 361, 361

Penner A.R., 2017, Astrophys. Space Sci., 362, 80

Penner A.R., 2018, Gravitational Anti-Screening as an Alternative to Dark Matter, in Research Advances in Astronomy, ed. N. Mehler. (NY, NY: Nova US), 1

Penner A.R., 2020, Astrophys. Space Sci., 365, 65

Penner A.R., 2022, Classical and Quantum Gravity, 39, 075001

Petersen S.D., 1979a, Astrophys. J. Suppl. Ser., 40, 527

Petersen S.D., 1979b, Astrophys. J., 232, 20

Pittordis C., Sutherland, W.,2023, arXiv:2205.02846v3

Planck Collaboration, 2020, arXiv:1807.06209

Rosan M., Ghafourian N., Kasfi T., Banik I.,Haslbauer M., Cuomo V., Famaey B., Kroupa P., 2021, arXiv:2106.10304v3

Sanders R.H., 2003, MNRAS, 342-3, 901

Sanders R.H., 2014, Can. J. Phys., 93-2, 126

Scarpa R., Falomo R., Treves A., 2022, arXiv:2202.13766v1

Schweizer L.Y., 1987a, Astron. Astrophys. Suppl. Ser., 64, 411

Schweizer L.Y., 1987b, Astron. Astrophys. Suppl. Ser., 64, 427

Turner E.L., 1976a, Astrophys. J., 208, 20

Turner E.L., 1976b, Astrophys. J., 208, 304

Turner E.L., Ostriker J.P., 1977, Astrophys. J. 217, 24

van Moorsel G.A., 1982, Astron. Astrophys. 107, 66

van Moorsel G.A., 1983a, Astron. Astrophys. Suppl. Ser., 53, 271

van Moorsel G.A., 1983b, Astron. Astrophys. Suppl. Ser., 54, 1

van Moorsel G.A., 1983c, Astron. Astrophys. Suppl. Ser., 54, 19

van Moorsel G.A., 1987, Astron. Astrophys. 176, 13

White S.D., 1981, MNRAS, 195, 1037

White S.D., Huchra J., Latham D., Davis M., 1983, MNRAS, 203, 701

Wu X., Kroupa P., 2015, MNRAS, 446-1, 330

Zhao H., Li B., Bienayme O., 2010, Physical Review D, 82, 103001

Zwicky F., 1933, Helv. Phys. Acta,, 6, 110